On the origin of structural phase transitions in Ni-rich LiNi0.8Co0.1Mn0.1O2 with lithiation/delithiation: a first-principles study

Liang-Yin Kuo,†‡ Olivier Guillon,‡ and Payam Kaghazchi*‡

† Physikalische und Theoretische Chemie, Freie Universität Berlin, Arnimallee 22, Berlin, D-14195, Germany

‡ Forschungszentrum Jülich GmbH, Institute of Energy and Climate Research, Materials Synthesis and Processing (IEK-1), Jülich, D-52425, Germany

*Payam Kaghazchi, E-Mail: p.kaghazchi@fz-juelich.de

ABSTRACT: In this work, non-monotonic lattice parameter changes and phase transitions in $Li_xNi_{0.8}Co_{0.1}Mn_{0.1}O_2$ (Li*x*NCM811) during delihtiation are studied by combining an extensive set of electrostatic and density functional theory (DFT) calculations. For the first time, we simulated and explained the reason behind the experimentally-observed hexagonal to monoclinic (H−M) phase transition at $x = 0.50$ as well as O3 → O1 phase transition at $x = 0.00$ in this system. By analyzing atomic and electronic structures of ions at each layer it is shown that the H−M phase transition is driven by the Jahn-Teller (J−T) distortion effect. Moreover, it was found that the O3 → O1 phase transition is driven by electrostatic forces. This study also shows that the oxidation of Ni cations as well as their nature of bonds with O are not similar at different Ni/Ni, Ni/Co and Ni/Mn layers. We also found that the significant decrease in the *c* lattice parameter for low values of *x* is due to the disappearance of J−T distortions as well as large covalent O−Ni bonds and oxidation of O, and more importantly sliding of O−TM−O layers with respect to each other.

KEYWORDS. Li-ion battery, Ni-rich NCM, Simulation, Phase transition, J−T distortion.

Introduction

There is an urgent need to design cathode materials with high energy densities, low costs, and long calendar life for Li-ion batteries (LIBs) in electric vehicles. The well-known $LiCoO_2$ (LCO) cathodes are unsuitable to meet the aforementioned requirements due to their low energy densities, high cost of Co, and poor structural and thermal stability. The first drawback is related to the low operating voltage (~4.3 V) as well as specific capacity.[1,2] The reason of the constrained voltage is a structural instability (*i.e.*, severe phase transition) induced by extraction of more than half Li contents during charging.[3-5] The O3 → O1 phase transitions at low Li contents decrease the Li diffusivity leading to the capacity fading upon cycling.[6] In recent years, a large number of layered cathode materials in which Co was replaced by other active transition metals (TMs) has been investigated.[7-10] Substitution of Co by Ni and Mn cations to form $LiNi_xCo_yMn_{1-x-y}O_2$ (NCMxy1-x-y) materials is one of the most interesting and practical approach to improve the capacity as well as energy density of cathodes. Moreover, Ni and Mn are cheaper than Co reducing the overall price of LIBs. NCM cathodes with high Ni contents are expected to increase the capacity of LIBs due to the fact that more Li ions can be extracted from $LiNiO_2$ (LNO) in comparison to LCO when charging at the same voltage.[3] Thus, Ni-rich NCM materials are highly interesting for electric vehicles. For this reason, for example, NCM811 has been widely studied.[11-13] The substitution of Ni by Mn cations reduces the number of Ni^{4+} upon charging and therefore the chemical reaction between the surface of cathode with electrolyte can be suppressed.[3,14] Although Co cation can stabilize the atomic structures of NCM, the influence on thermal stability for NCM cathodes is smaller than the Mn cation. Nevertheless, the small amount of Co and Mn cations compared to the Ni content in Ni-rich NCM can hardly prevent phase transitions and lattice parameters change leading to a poor cycle life of these cathodes during charging/discharging.

The structural instability of NCM cathodes originates mainly from a large anisotropic lattice-parameters change in the half delithiated state as well as the O3 → O1 phase transition at high delithiation level. Upon delithiation (charging), the lattice parameters *a* and *b* of Li*x*NCM811 shrink for $1.00 > x > 0.25$,[15-17] and then they slightly expand for $0.25 > x$.[18] Whereas the lattice parameter *c* initially increases for $1.00 > x > 0.50$, and then it decreases for $0.25 > x$.[12,19,20] The phase transitions in Ni-rich NCM cathodes have been reported to be similar to those of

LNO which undergoes hexagonal to monoclinic (H1 → M), monoclinic to hexagonal (M → H2), and hexagonal to hexagonal (H2 → H3) transitions with delithitation.[21, 22] Due to the hexagonal structure with Li and TM cations occupying in octahedral sites as well as oxygen layers stacked in an $(ABC)n$ sequence, the phase is also labelled as O3.[23] However, the fully-delithiated structure in which the oxygen layer stacking changes to an $(AB)_n$ sequence is labelled as O1 phase.[23] Moreover, an intermediate phase (so-called H1-3) with alternating layers of O3 and O1 phases at low lithium contents has been proposed as well[3,23].

In this work, we used electrostatic analysis and density functional theory (DFT) calculation to compute lattice parameters change as well as atomic and electronic structures for NCM811. In particular, we simulated the hexagonal to monoclinic (hereafter called H → M) phase transition at x = 0.50, which has been reported by experimentalists for Ni-rich cathodes[15,16,34] but not simulated so far. In addition, we explained a possible reason for the O3 → O1 phase transition at low Li contents.

Methods

Spin-polarized DFT calculations were performed with the Projector Augmented-Wave (PAW)[35] pseudopotential method implemented in the Vienna Ab initio Simulation Package (VASP) code.[36] The SCAN (strongly constrained and appropriately normed) functional [31] was employed to approximate the exchange-correlation (XC) energy for all DFT calculations on atomic and electronic structures, while the PBE functional[28] was applied to explore the most favorable i) Li arrangements that were predetermined by total Coulomb-energy calculations as well as ii) TM arrangements. Total Coulomb-energy (E_C) calculations on various possible combinations were carried out using the supercell code.[37] The $Li_xNi_{0.8}Co_{0.1}Mn_{0.1}O_2$ (LixNCM811) bulk with a space group of $R\bar{3}m$ was modelled using 2×2×1 (*e.g.*, fully lithiated case: $Li_{12}Ni_{10}Co_1Mn_1O_{24}$) and 4×4×1 (*e.g.*, fully lithiated case: $Li_{48}Ni_{40}Co_4Mn_4O_{96}$) supercells. The former was used to calculate E_C for x = 0.75, x = 0.50, and x = 0.25, while the latter was considered for calculating E_C for x = 0.125 and to perform all DFT calculations for $1.00 \geq x \geq 0.00$. To calculate E_C, all possible arrangements of 9Li ions in 12Li sites for Li0.75NCM811 and 3Li ions in 12Li sites for Li0.25NCM811, namely $\frac{12!}{9!3!} = 220$ configurations, were considered. For both Li0.50NCM811 and Li0.125NCM811, we also considered all possible combinations, namely: $\frac{12!}{6!6!} = 924$ and $\frac{48!}{6!42!} = 12271516$, respectively. According to our recent study on NCM111,[33] E_C calculations with an average charge value for TMs and formal charge states for Li and O give reasonable Li arrangements. Thus, we used charge states of 3.25+, 3.50+, 3.75+, and 3.875+ for each TM cation at x = 0.75, x = 0.50, x = 0.25, and x = 0.125, respectively. For all Li concentrations, the charge value of 1+ for Li ions and 2− for O anions were considered. DFT calculations on atomic structures and lattice parameters were carried out using a Gamma-centred 2×2×1 k-point mesh and an energy cutoff of 500 eV as well as an energy and force convergence criterion of 10^{-4} eV and 10^{-3} eVÅ^{-1}, respectively. Atomic positions and unitcell optimization were performed without applying any constraint. Density of states (DOS), spin density difference (SDD), Bader charges (BCs), and magnetizations were calculated using a Gamma-centred 4×4×1 k-point mesh with an electronic and force convergence criterion of 10^{-6} eV and 10^{-5} eVÅ^{-1}, respectively. Atomic structures and SDD were visualized with the VESTA program.[38]

Results and Discussion

To find the most favorable arrangement of TMs, we performed an extensive number of DFT-PBE calculations. A total number of 71 configurations in which Mn and Co cations at three O−TM−O layers with various neighbors and stacking were located was considered. In the lowest-energy structure (see Fig. S1), Co and Mn prefer occupying different layers where Ni cations are their nearest neighbors, *i.e.*, clustering of Mn or Co is not favorable. Note that every third O−TM−O layer contains only Ni cations. The determined structure is similar to that reported by the DFT-PBE+U study of Lim *et al.*[39] Hereafter, the Ni layer without any Co and Mn is called Ni/Ni layer, while the layers with Ni and Co or Ni and Mn cations are called Ni/Co or Ni/Mn layers, respectively.

With the determined structure of Li1.00NCM811, we then performed E_C calculation to explore the most favorable arrangement of Li ions in Li sites for various Li concentrations x in LixNCM811. Computed E_C values of the 50 topmost favorable configurations as well as DFT-PBE-calculated total energies (E_{tot}) of 10 configurations with the lowest E_c are illustrated in Fig. S2 (a). It is found that the most favorable structures of x = 0.75 and x = 0.25 possess well-ordered hexagonal arrangements of Li ions at each layer. However, for x = 0.50 and x = 0.125, the Li ions arrange with a rectangular symmetry at each Li layer (Fig. S2 (b)).

Calculated lattice parameters with DFT-SCAN are illustrated in Fig. 1. The DFT-SCAN results show that a value shrinks for

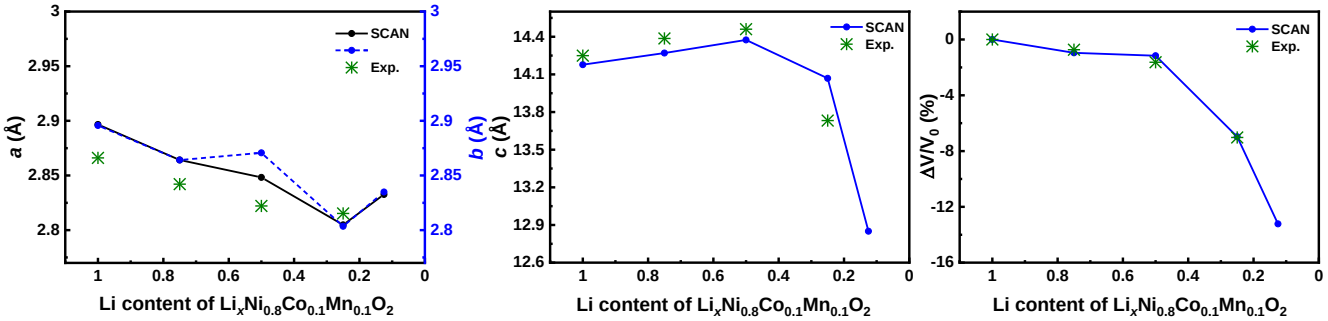

Figure 1. Referenced variation of lattice parameters and unit cell volume with DFT-SCAN functional. Experimental results by Kondrakov *et al.*[19] are included for comparison.

1.00 > x > 0.25, and then expands for 0.25 > x. However, b decreases for 1.00 > x > 0.75, and then it increases for 0.75 > x > 0.50, and finally it shows a similar variation to a. The deviation between a and b at x = 0.50 is the indication of the H → M phase transition. As will be discussed later in this article, this behavior at x = 0.50 is purely governed by the J−T distortion. Figure 1 indicates that the lattice parameter c increases for 1.00 > x > 0.50, and then it decreases for 0.50 > x. Size of c decreases strongly for 0.25 > x. Moreover, we find that the volume always shrinks during delithiation, *i.e.*, x = 1.00 → x = 0.125. The absolute values of a, c, and V calculated by the SCAN functional are in fair agreement with the experimental results. For example, by using the DFT-SCAN functional, $\Delta V/V_0$ is estimated to decrease by −6.97 % for x = 1.00 → x = 0.25 which is very close to the measurement by Kondrakov *et al.*[19] showing the value changes of −7.02 %. Moreover, the SCAN functional predicts reasonably the magnetization. The better performance of SCAN to predict atomic and electronic structures compared to PBE and PBE+U has also been reported for LCO,[32] LNO,[32] LMO,[32] and NCM111.[33]

The lattice parameter a of NCM811 experiences a larger maximum contraction (3.17 %) than that of NCM111 (1.36 %) when Li concentration decreases. Moreover, the expansion of a for NCM811 (0.99 %) is larger than that for NCM111 (0.95 %) at low Li concentrations, namely 0.25 > x and 0.33 > x, respectively. This is because larger number of Co cations per layer is oxidized in NCM811 than NCM111 causing a stronger electrostatic repulsion between Co and other cations in the former case. The initial contraction of c for x = 0.50 → 0.25 in NCM811 (Δc = −2.13 %) is 0.77 % larger than that for x = 0.50 → 0.33 in NCM111. However, the contraction of c is 0.24 % smaller in NCM811 (Δc = −8.66 %) than NCM111 at lower Li contents.[33]

To understand the variation of lattice parameters with delithiation, we computed spin density difference (SDD), number of unpaired spins (NUS), Bader charges (BCs), and density of state (DOS) (Fig. 2 and Figs S3-S6) followed by computed average projected O−TM−O intralayer (d_1) and O−TM−O interlayer (d_2) distances (Fig. 4).

Li1.00NCM811 (Fig. 2 and Tab. S1 in SI)
<u>*Ni/Ni layer*</u> The computed averaged absolute value of NUS, $|\overline{\mathrm{NUS}}|$ = 0.90, for 16Ni indicates the charge states of 16Ni cations to be 3+. The DOS plot shows three up- and down-spin peaks of t_{2g} (Ni) indicating paired electrons occupying d_{xy}, d_{yz}, and d_{xz} orbitals of Ni cations. In addition, up-spin SDD features (in yellow) on Ni and a single up-spin peak at −1.12 eV ≤ $\varepsilon - \varepsilon_F \leq -0.07$ eV in DOS plot indicate most likely an unpaired electron in the d_{z^2} orbital of Ni cations. A similar occupation of d_{z^2} orbitals of Ni^{3+} has also been proposed by Radin *et al.*[3] for Ni-based cathodes. The DOS plot demonstrates that the e_g states of Ni cations are close to the fermi level and, therefore, electrons can be easily removed from these states with a further delithiation. The charge states of cations can also be understood by analyzing the TM−O bond lengths. The average axial and equatorial Ni−O bond lengths of $\bar{d}^{\mathrm{Ni}}_{\mathrm{axial}}$= 2.17 Å and $\bar{d}^{\mathrm{Ni}}_{\mathrm{equatorial}}$ = 1.91 Å, respectively, at the Ni/Ni layer demonstrate the Jahn-Teller (J−T) distortion which we define it as $\bar{d}^{\mathrm{Ni}}_{\mathrm{axial}}/\bar{d}^{\mathrm{Ni}}_{\mathrm{equatorial}}$ = 1.14.

<u>*Ni/Co layer*</u> The value of $|\overline{\mathrm{NUS}}|$ = 0.93 is estimated for 12Ni cations indicating formation of $12Ni^{3+}$. The DOS plot also shows the occupation of e_g (Ni) close to the ε_F. However, the J−T distortion in Ni^{3+}−O octahedra is suppressed due to the substitution of 4Ni by 4Co since the computed $\bar{d}_{\mathrm{axial}}/\bar{d}_{\mathrm{equatorial}}$ (= 1.07) for 12Ni cations at this layer is smaller than that in the Ni/Ni layer. A small distortion of $\bar{d}_{\mathrm{axial}}/\bar{d}_{\mathrm{equatorial}}$ = 1.03 for Co^{3+}−O octahedra is probably induced by the J−T distortion of $12Ni^{3+}$−O octahedra. The calculated $|\overline{\mathrm{NUS}}|$ value of 0.07 as well as more down-spin than up-spin states (according to DOS and SDD plots) indicate the charge states of Co cations are slightly lower than 3+ (*i.e.*, a partial occupation of e_g states). The DOS plot in Fig. 2 (f) illustrates three large up- and down-spin peaks below the Fermi level confirming occupation of t_{2g} (Co) orbitals (d_{xy}, d_{yz}, and d_{xz}) of Co cations with (almost) paired electrons. Furthermore, the top part of d states of Co cuts through to the fermi level showing their tendency to be depleted with delithiation.

<u>*Ni/Mn layer*</u> The $|\overline{\mathrm{NUS}}|$ values of 1.06 and 1.34 are obtained for 8Ni and 4Ni. This indicates that upon the Mn → Ni substitution, $8Ni^{3+}$ cations undergo a small reduction, while 4Ni cations experience relatively larger reductions to $4Ni^{(3-\Delta1)+}$. This can also be seen by comparing DOS plots in Figs 2 (d) and 2 (e) showing a slightly larger occupied states below the Fermi level for $4Ni^{(3-\Delta1)+}$. Therefore, we conclude that only a small fraction of Ni cations in NCM811 has a charge state smaller than 3+. It has also been reported by Flores *et al.* that Ni^{3+} is dominant in the fully-lithiated NCM811.[40] The BCs analysis for Ni at different layers (Fig. 2) does not provide any clear evidence for the presence of 4 reduced Ni^{3+}, *i.e.*, $Ni^{(3-\Delta1)+}$, at the Ni/Mn layer. However, our total Coulomb-energy calculation indicates if a $4Ni^{3+}$ → $4Ni^{2+}$ reduction occurs (to keep the overall charge neutrality of the system) after a $4Mn^{4+}$ → $4Ni^{3+}$ substitution, the $4Ni^{2+}$ cations prefer to be at the Ni/Mn layer rather than at the other layers. The SDD features on Mn cations are larger than those on all types of Ni cations which qualitatively shows a charge state of Mn^{4+}. The calculated $|\overline{\mathrm{NUS}}|$ value of 2.79 for Mn confirms this result. The DOS plot also shows two significant up-spin peaks and shoulders at $-2.71\ \mathrm{eV} \leq \varepsilon - \varepsilon_F \leq -0.96\ \mathrm{eV}$ as well as a small broad up-spin peak at −3.94 eV of t_{2g}(Mn). The smaller J−T distortion of $8Ni^{3+}$ ($\bar{d}_{\mathrm{axial}}$ / $\bar{d}_{\mathrm{equatorial}}$ = 1.07) compared to $16Ni^{3+}$ in the Ni/Ni layer is due to the existence of 4 J−T inactive $Ni^{(3-\Delta1)+}$−O and $4Mn^{4+}$−O octahedra. The alleviation of J−T distortion of Ni due to the substitution of Ni by Co and Mn has also been reported by Kondrakov *et al.*[19] Calculated $|\overline{\mathrm{NUS}}|$ values of 1.41, 0.76, 0.06, and 2.67 have been reported by Dixit *et al.*[14] for Ni^{2+}, Ni^{3+}, Co^{3+} and Mn^{4+} for the fully-lithiated NCM811. With their DFT-PBE calculations, they found a small contribution of Ni^{4+} with $|\overline{\mathrm{NUS}}|$ of 0.10 at full lithiated state which is not observed in our work. This might be due to the different computational parameters, supercell size, and, more importantly, the type of XC functional. The blue features of SDD on O anions (*e.g.*, O78) close to Mn are smaller (due to a partial up-spin electron transfer to O78) than those (*e.g.*, O6) close to Ni in the Ni/Ni layer. This might show that O anions in the Ni/Mn layer are slightly more reduced, which can also be confirmed from BCs (Fig. 2 (l)). This is in line with DFT-PBE calculation by Dixit *et al.*[14] reporting that with an increase of Ni content with respect to Mn (NCM424 vs NCM811) more oxidation occurs on O anions. Furthermore, we found that there is scatter in the NUS and Bader charge values of Ni and O

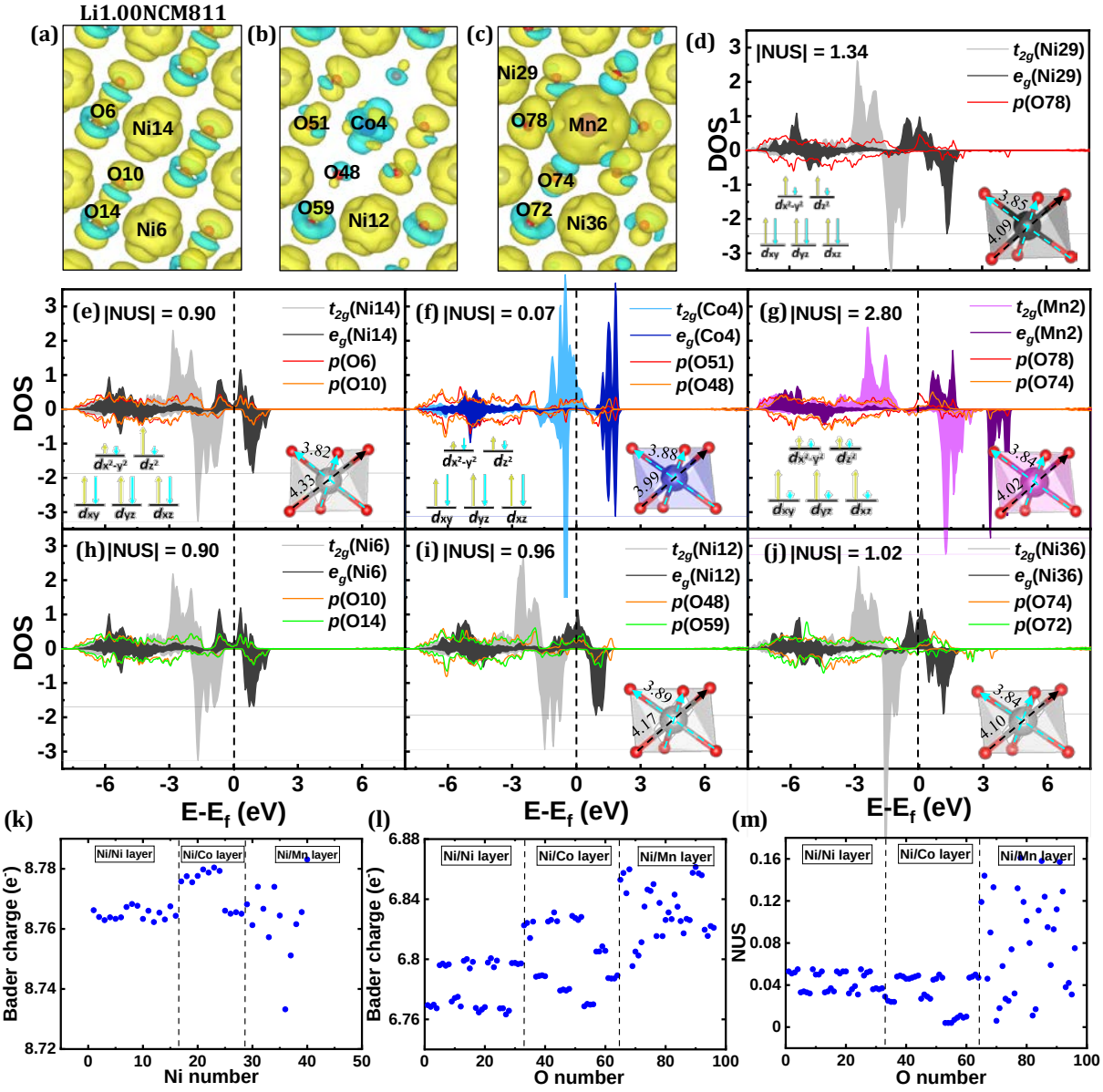

Figure 2. (a-c) Spin density difference (SDD), **(d-j)** Density of states (DOS) with local number of unpaired spin (NUS) on Ni, Co, and Mn cations, respectively, as well as their bond lengths with O and proposed electronic configurations, **(k-l)** Bader charges of Ni and O, and **(m)** NUS of O anions for Li1.00NCM811. The yellow and blue features in SDD plots represent up- and down-spin electrons. A SDD isosurface of 0.004 eV/A^3 was used for all structures. The atom numbers of Ni, Co, Mn, and O in SDD and DOS plots are the same as those in NUS and Bader charge analysis.

at the Ni/Mn layer. This is probably due to the existence of Mn^{4+} cations and their interaction with other ions at this layer. For example, for x = 1.00, only Ni^{3+} cations exist in the Ni/Ni and Ni/Co layers, but 4Ni cations at the Ni/Mn layer have charge states close to 2+ and the rest Ni cations possess a charge state of 3+.

Li0.75NCM811 (Fig. S3, and Tab. S2 in SI) *Ni/Ni layer* When 25 % of the Li content is removed from Li1.00NCM811, we found changes in $|\overline{NUS}|$ values of 0.90 → 0.45 for 4Ni, 0.90 → 0.53 for 4Ni, and 0.90 → 0.88 for 8Ni which may show a $8Ni^{3+} \rightarrow 8Ni^{3.5+}$ oxidation for x = 1.00 → x = 0.75. As will be discussed in the following, SDD, DOS, and BCs confirm oxidation of these Ni cations, but they do not provide any quantitative result for the amount of increase in the charge states of Ni cations: i) the SDD features on the 8Ni cations are smaller than those in the case of x = 1.00; ii) the DOS plot indicates that part of the e_g peak at -1.12 eV $\leq \varepsilon - \varepsilon_F \leq -0.07$ eV in Li1.00NCM811 is located above the Fermi level in Li0.75NCM811; and iii) increases in the averaged Bader charge ($\overline{BC}$) of the aforementioned Ni cations (with respect to those in Li1.00NCM811) is calculated to be 0.14 |e|, 0.05 |e|, and 0.06 |e|, respectively. However, our total Coulomb-energy calculations indicate that the $4Ni^{3+} \rightarrow 4Ni^{4+}$ oxidation is more favorable than $8Ni^{3+} \rightarrow 8Ni^{3.5+}$ at the Ni/Ni layer. In addition, the calculated $\bar{d}_{axial}/\bar{d}_{equatorial}$ is 1.00, 1.05, and 1.08 for those Ni cations with the $\overline{BC}$ changes of 0.14 |e|, 0.05 |e|, and 0.06 |e|, respectively. We, therefore, propose that 8Ni cations undergo

oxidation but 4 of them are oxidized to higher extent (*i.e.*, $4Ni^{3+} \rightarrow 4Ni^{(4-\Delta 2)+}$, and $4Ni^{3+} \rightarrow 4Ni^{(4-\Delta 3)+}$ where $\Delta 2 < \Delta 3$).

Ni/Co layer A decrease of $|\overline{NUS}|$ of 0.93 → 0.07 for 4Ni cations (out of 12) and an increase of 0.09 |e| in their $\overline{BC}$ for $x = 1.00 \rightarrow x = 0.75$ show their oxidation from $4Ni^{3+}$ to $4Ni^{4+}$. A large decrease of up-spin features on these 4Ni can also be seen in the SDD plot. The calculated $\bar{d}_{axial}/\bar{d}_{equatorial}$ for these $4Ni^{4+}$ is 1.06 and not 1. This is most likely due to the fact that the $4Ni^{4+}$ cations are located directly between Co cations (see Fig. S7 in SI). In this case, Ni^{4+} cations cannot pull axial O48 and O48' anions from Co^{3+} away. This is because Co–O bonds have been reported to be stronger than that of Ni–O bonds.[41-43] The other 8Ni cations show $|\overline{NUS}|$ changes of 0.93 → 0.94 and a small increase of $\overline{BC}$ of 0.04 |e| for $x = 1.00 \rightarrow x = 0.75$ indicating that their charge states are preserved to be 3+. Calculated SDD and DOS as well as $|\overline{NUS}|$ changes of 0.07 → 0.04, $\overline{BC}$ increases of 0.04 |e|, and $\bar{d}_{axial} / \bar{d}_{equatorial}$ = 0.99 show a very small oxidation in Co^{3+} cations.

Ni/Mn layer The $|\overline{NUS}|$ value of $4Ni^{(3-\Delta 1)+}$ cations decreases from 1.34 to 0.87 when $x = 1.00 \rightarrow x = 0.75$. A shift of e_g states above the Fermi level in $x = 0.75$ compared to $x = 1.00$ in the calculated DOS for these 4Ni cations confirm the following oxidation: $4Ni^{(3-\Delta 1)+} \rightarrow 4Ni^{3+}$. However, the $\overline{BC}$ variations do not provide any conclusive result on the oxidation of these Ni cations. Because of this and due to the smaller decrease in $|\overline{NUS}|$ of these 4Ni compared to Ni cations at the Ni/Co layer, we propose an oxidation smaller than 1 for these 4Ni cations for which the J–T distortion is estimated to be $\bar{d}_{axial}/\bar{d}_{equatorial}$ = 1.06. The other $8Ni^{3+}$ cations show a $|\overline{NUS}|$ change of 1.06 → 0.96 and a $\overline{BC}$ change of 0.02 |e| indicating no significant change in their charge states as well. Both Bader charge analysis and NUS values show that O anions at the Ni/Mn layer are slightly oxidized for $x = 1.00 \rightarrow x = 0.75$ (see Fig. S8 in SI). Calculated SDD and DOS plots as well as $|\overline{NUS}|$ variations of 2.79 → 2.78, $\overline{BC}$ changes of − 0.03 |e|, and average $\bar{d}_{axial}/\bar{d}_{equatorial}$ = 1.03 demonstrate only a small reduction for Mn cations.

Li0.50NCM811 (Fig. S4 and Tab. S3 in SI)
Ni/Ni layer Upon a further delithiation ($x = 0.75 \rightarrow x = 0.50$), SDD features on $4Ni^{(4-\Delta 3)+}$ cations that have a decrease of 0.53 → 0.02 in $|\overline{NUS}|$ and an increase of 0.05 |e| → 0.16 |e| in $\overline{BC}$ indicate an oxidation of $4Ni^{(4-\Delta 3)+} \rightarrow 4Ni^{4+}$. The already partially oxidized $4Ni^{(4-\Delta 2)+}$ cations at $x = 0.75$ undergo $|\overline{NUS}|$ changes of 0.45 → 0.01 and $\overline{BC}$ changes of 0.14 |e| → 0.17 |e|. This means that they are also further oxidized (compared to $x = 0.75$) and become $4Ni^{4+}$. The SDD features of the rest 8Ni cations remain almost unchanged. A decrease of $|\overline{NUS}|$ of 0.88 → 0.82 and $\overline{BC}$ changes of 0.06 |e| → 0.07 |e| are obtained for these 8Ni cations for $x = 0.75 \rightarrow x = 0.50$ indicating that they are still Ni^{3+}. The calculated $\bar{d}_{axial} / \bar{d}_{equatorial}$ of 1.02 for $8Ni^{4+}$ is most likely because of the change in Ni–O bond lengths due to the neighboring ions and Li vacancies. However, the higher value of 1.04 for $\bar{d}_{axial}/\bar{d}_{equatorial}$ in $8Ni^{3+}$ is probably due to the local J-T effect. A partial hybridization between p(O) and d(Ni^{4+}) states at -7.02 eV ≤ $\varepsilon - \varepsilon_F \leq -3.84$ eV is observed in the DOS plots indicating a slight O–Ni^{4+} covalency behavior.

Ni/Co layer Larger up-spin features for 8Ni cations in SDD plots with $|\overline{NUS}|$ changes of 0.94 → 0.57, and an increase of $\overline{BC}$ of 0.04 |e| → 0.09 |e| for $x = 0.75 \rightarrow x = 0.50$ indicates partial oxidation of $8Ni^{3+} \rightarrow 8Ni^{(4-\Delta 4)+}$. Whereas the rest 4Ni cations that have been already oxidized to Ni^{4+} for $x = 1.00 \rightarrow x = 0.75$ also undergo additional small oxidation. This can be concluded from $|\overline{NUS}|$ changes of 0.07 → 0.01 and an increase in $\overline{BC}$ of 0.09 |e| → 0.15 |e| when $x = 0.75 \rightarrow x = 0.50$. The J–T distortion of these 4 fully-oxidized Ni^{4+} is alleviated for which $\bar{d}_{axial}/\bar{d}_{equatorial}$ is calculated to be 1.01 (1.06 for $x = 0.75$). The SDD changes on Co cations show partial oxidations of Co cations as well. An increase of $|\overline{NUS}|$ of 0.04 → 0.43 as well as a small shift of up- and down-spin states above the fermi level in DOS plots and an oxidation of 0.04 |e| → 0.05 |e| for Co cations when $x = 0.75 \rightarrow x = 0.50$ confirm their partial oxidation to $Co^{(3+\zeta 1)+}$. The unexpected partial oxidations of Ni and Co are most likely due to the hexagonal-monoclinic (H–M) phase transition occurring at $x = 0.50$. The continuous partial oxidation of Co cations has also been reported by Saadoune *et al.*[44] and Chebiam *et al.*[45]

Ni/Mn layer The sphere-like up-spin features on Ni cations in SDD plots, and $|\overline{NUS}|$ changes of 0.87 → 1.59 with $\overline{BC}$ decreases of 0.03 |e| → −0.03 |e| indicate reduction of $4Ni^{3+} \rightarrow 4Ni^{2+}$. The $|\overline{NUS}|$ changes of 0.96 → 0.02 and $\overline{BC}$ variations of 0.02 |e| → 0.12 |e| for other 8Ni cations show their oxidation, *i.e.*, $8Ni^{3+} \rightarrow 8Ni^{4+}$. The $\bar{d}_{axial}/\bar{d}_{equatorial}$ of 0.96 and $\bar{d}_{axial}/\bar{d}_{equatorial}$ of 1.02 are obtained for Ni^{2+} and Ni^{4+}, respectively. Furthermore, our total Coulomb-energy analysis indicates that the presence of $4Ni^{2+}$ and $8Ni^{4+}$ at the Ni/Mn layer is electrostatically more favorable than that of $8Ni^{3+}$ and $4Ni^{4+}$ at the Ni/Mn layer. The DOS plot shows the largest spin splitting for Ni^{2+} cations and smallest for Ni^{4+} at the Ni/Mn layer. An exchange splitting of Ni for NCM523 has also been reported by Dixit *et al.* with DFT-PBE+U calculation.[25] Fig. S4 (c) shows no significant changes in the SDD of Mn cations. However, the increase in $|\overline{NUS}|$ of 2.78 → 3.07, $\overline{BC}$ of −0.03 |e| → 0.06 |e| on Mn and increase of BCs on O (see Fig. S8 in SI) show that Mn and O are slightly oxidized.

Li0.25NCM811 (Fig. S5 and Tab. S4 in SI)
Ni/Ni layer When $x = 0.50 \rightarrow x = 0.25$, besides $8Ni^{4+}$, further 4 (out of 8) Ni^{3+} cations undergo a decrease of $|\overline{NUS}|$ of 0.82 → 0.02 and $\overline{BC}$ increases of 0.07 |e| → 0.16 |e| indicating oxidation of $4Ni^{3+} \rightarrow 4Ni^{4+}$. The J–T distortion is supressed for these Ni cations for which $\bar{d}_{axial} / \bar{d}_{equatorial}$ is computed to be 1.01. However, the rest $4Ni^{3+}$ cations preserve their 3+ charges since only a small decrease of 0.82 → 0.73 and an increase of 0.07 |e| → 0.10 |e| are calculated for their $|\overline{NUS}|$ and $\overline{BC}$, respectively. The calculated average $\bar{d}_{axial}/\bar{d}_{equatorial}$ is 1.04 for these $4Ni^{3+}$ cations. The already oxidized $8Ni^{4+}$ cations for $x = 0.75 \rightarrow x = 0.50$, show also a small $|\overline{NUS}|$ decrease of 0.02 → 0.01 and a small $\overline{BC}$ reduction of 0.16 |e| → 0.15 |e| for $x = 0.50 \rightarrow x = 0.25$. This indicates a small change in charge states of these Ni cations. In addition, a more hybridization of O–Ni^{4+} states (at -5.62 eV ≤ $\varepsilon - \varepsilon_F \leq -4.31$ eV at $x = 0.25$) in $x = 0.25$ compared to $x = 0.50$ is observed showing an increase in the O–Ni covalency.

Ni/Co layer A decrease of $|\overline{NUS}|$ of 0.57 → 0.00 and a $\overline{BC}$ variation of 0.09 |e| → 0.14 |e| for 4 out of $8Ni^{(4-\Delta 4)+}$ cations indicates a full oxidation of these cations, *i.e.*, $4Ni^{(4-\Delta 4)+} \rightarrow 4Ni^{4+}$, when $x = 0.50 \rightarrow x = 0.25$. The other $4Ni^{(4-\Delta 4)+}$ cations show a

|$\overline{\text{NUS}}$| decrease of 0.57 → 0.28 and an increase of $\overline{\text{BC}}$ of 0.09 |e| → 0.16 |e|. This result indicates a slight oxidation of these 4Ni cations to $4Ni^{(4-\Delta5)+}$. In addition, we observe a slightly larger SDD on these $Ni^{(4-\Delta5)+}$ cations compared to the aforementioned $4Ni^{4+}$ cations meaning that they are further oxidized, but not completely. The already oxidized $4Ni^{4+}$ cations undergo a |$\overline{\text{NUS}}$| change of 0.01 → 0.02 and a $\overline{\text{BC}}$ variation of 0.15 |e| → 0.13 |e| for $x = 0.50 \rightarrow x = 0.25$. The decrease of SDD features as well as an increase of |$\overline{\text{NUS}}$| of 0.43 → 0.46 and $\overline{\text{BC}}$ changes of 0.05 |e| → 0.06 |e| indicate further partial oxidation of Co cations for $x = 0.50 \rightarrow x = 0.25$. Moreover, the DOS plots also demonstrate a hybridization of O and Ni at -7.33 eV $\leq \varepsilon - \varepsilon_F \leq -3.78$ eV confirming partial covalency of O–Ni bonds.

<u>*Ni/Mn layer*</u> Shrinking of SDD as well as a |$\overline{\text{NUS}}$| decrease of 1.59 → 0.28 and an increase of $\overline{\text{BC}}$ of −0.03 |e| → 0.15 |e| of $4Ni^{2+}$ for $x = 0.50 \rightarrow x = 0.25$ indicate their oxidation from $4Ni^{2+}$ to $4Ni^{(4-\Delta6)+}$. However, an increase of down-spin SDD features for other $8Ni^{4+}$ as well as an oxidation of 0.12 |e| → 0.14 |e| in $\overline{\text{BC}}$ for $x = 0.50 \rightarrow x = 0.25$ showing that the 8Ni cations are partial oxidized. However, an increase of |$\overline{\text{NUS}}$| of 0.02 → 0.22 is calculated for these $8Ni^{4+}$ cations where a large hybridization of O and Ni is observed at -7.18 eV $\leq \varepsilon - \varepsilon_F \leq -4.8$ eV when the backward monoclinic-hexagonal (M–H) phase transition occurs. The disappearance of topmost up-spin states of e_g(Mn) in the DOS plot as well as a |$\overline{\text{NUS}}$| change of 3.07 → 2.62 and an oxidation of 0.06 |e| → 0.07 |e| (in $\overline{\text{BC}}$) demonstrate that Mn cations are also slightly oxidized. The p(O)– e_g (Ni) hybridization for $Ni^{(4-\Delta6)+}$ is less for O–Ni at this layer compared to Ni at the other layers.

Li0.125NCM811 (Fig. S6 and Tab. S5 in SI) <u>Ni/Ni layer</u> When $x = 0.25 \rightarrow x = 0.125$, $4Ni^{3+}$ cations undergo a decrease in |$\overline{\text{NUS}}$| of 0.73 → 0.11 with a $\overline{\text{BC}}$ increase of 0.10 |e| → 0.16 |e| indicating their oxidations: $4Ni^{3+} \rightarrow 4Ni^{4+}$. The already oxidized $12Ni^{4+}$ for $x = 0.50 \rightarrow x = 0.25$ experience only small changes in their |$\overline{\text{NUS}}$| (0.01 → 0.20) and $\overline{\text{BC}}$ increases slightly (0.151 |e| → 0.146 |e|) for $x = 0.25 \rightarrow x = 0.125$. The DOS plots clearly show a large hybridization between p(O) and e_g(Ni) at -7.40 eV $\leq \varepsilon - \varepsilon_F \leq -2.18$ eV. Due to the combined covalent-ionic nature of bonding between p(O)– e_g (Ni), the SDD plot becomes difficult to analyze.

<u>Ni/Co layer</u> A transition from incomplete to complete oxidation occurs for $4Ni^{(4-\Delta5)+}$ cations when $x = 0.25 \rightarrow x = 0.125$ as the |$\overline{\text{NUS}}$| value becomes very small (0.28 → 0.07) and the $\overline{\text{BC}}$ increases (0.16 |e| → 0.18 |e|). The already oxidized $8Ni^{4+}$ cations for $x = 0.50 \rightarrow x = 0.25$ do not undergo significant oxidation or reduction. Considering an increase of |$\overline{\text{NUS}}$| of 0.46 → 0.50 and a large $\overline{\text{BC}}$ change of 0.06 |e| → 0.12 |e| as well as an increase of down-spin features on Co in SDD and a larger amount of down-spin states of t_{2g}(Co) below the fermi level, we propose that oxidation of Co cations (to $Co^{(3+\zeta2)+}$) occur at $x = 0.125$. The up- and down-spin splitting on Co in Fig. S6 (f) confirms this behavior. The DOS plot shows a greater hybridization for p(O)– e_g (Ni) at this Li concentration compared to $x = 0.25$, but the hybridization is smaller than that at the Ni/Ni layer. The p(O)–e_g(Co) covalency also increases compared to $x = 0.25$.

<u>Ni/Mn layer</u> The |$\overline{\text{NUS}}$| of the already oxidized $12Ni^{4+}$ ($4Ni^{(4-\Delta6)+}$ + $8Ni^{4+}$) decreases further (0.25 → 0.08) and their $\overline{\text{BC}}$ increases slightly (0.142 |e| → 0.143 |e|) for $x = 0.25 \rightarrow x = 0.125$. The DOS plots do not show a significant change in the covalent nature of p(O)–e_g(Ni) at this layer compared to $x = 0.25$. An increase of |$\overline{\text{NUS}}$| of 2.62 → 2.96 and $\overline{\text{BC}}$ reduction of 0.07 |e| → 0.04 |e| indicate the reduction of Mn. The DOS plot also shows an increase of down-spin state in t_{2g} (Mn) orbitals. Slight hybridization also occurs between p(O)–d(Mn) compared to $x = 0.25$.

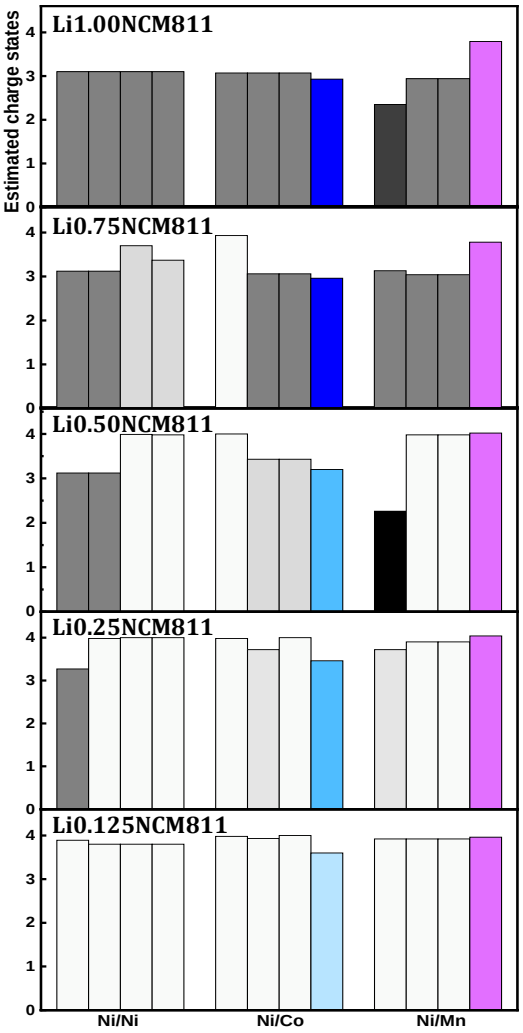

Figure 3. Variation of charge states of 40Ni, 4Co, and 4Mn at each layer of Li$_x$NCM811 with delithiation. Each bar represents 4 cations. Ni^{2+}, $Ni^{(3-\Delta1)+}$, Ni^{3+}, $Ni^{(4-\Delta)+}$, and Ni^{4+} are in black, dark grey, moderate gray, light grey and white, respectively. Co^{3+}, $Co^{(3+\zeta1)+}$,and $Co^{(4-\zeta2)+}$ are in dark blue, moderate blue, and light blue, respectively. Mn^{4+} is in purple.

Fig. 3 summarizes our results on the variation of charge states of 40Ni, 4Co, and 4Mn with delithiation (for $x = 1.00 \rightarrow x = 0.125$). For $x = 1.00$, 16Ni cations at the Ni/Ni layer and 12Ni with 4Co at the Ni/Co layer show a charge state of ~ 3+. Whereas, at the Ni/Mn layer, 4Ni cations are partially ($4Ni^{(3-\Delta1)+}$) and 8Ni are very slightly reduced to compensate for the $4Ni^{3+} \rightarrow 4Mn^{4+}$ replacement. Upon the delithiation of $x = 1.00 \rightarrow x = 0.75$, $4Ni^{3+}$ cations are oxidized (to $4Ni^{(4-\Delta2)+}$) but not completely, while additional $4Ni^{3+}$ cations are slightly oxidized (to $4Ni^{(4-\Delta3)+}$) at the Ni/Ni layer. $4Ni^{3+}$ cations at the Ni/Co layer

are completely oxidized. At the Ni/Mn layer, the incomplete oxidation of Ni cations is compensated by a partial oxidation of $4Ni^{(3-\Delta1)+}$ (to $4Ni^{3+}$). The charge states of Co and Mn remain almost unchanged. For the delithiation of $x = 0.75 \rightarrow x = 0.50$ upon which the H−M phase transition occurs, complete oxidations of partially oxidized Ni, namely $4Ni^{(4-\Delta2)+}$ and $4Ni^{(4-\Delta3)+}$, are observed at the Ni/Ni layer. Whereas small oxidations of $8Ni^{3+} \rightarrow 8Ni^{(4-\Delta4)+}$ and $4Co^{3+} \rightarrow 4Co^{(3+\zeta1)+}$ take place, respectively, at the Ni/Co layer. However, a reduction of $4Ni^{3+} \rightarrow 4Ni^{2+}$ and an oxidation of $8Ni^{3+} \rightarrow 8Ni^{4+}$ occur at the Ni/Mn layer. The Mn cations remain the same charge. For $x = 0.50 \rightarrow x = 0.25$, further $4Ni^{3+}$ undergo an oxidation to $4Ni^{4+}$ at the Ni/Ni layer. At the Ni/Co layer, $4Ni^{(4-\Delta4)+}$ are fully oxidized to $4Ni^{4+}$, while the rest $4Ni^{(4-\Delta4)+}$ are partially oxidized to $4Ni^{(4-\Delta5)+}$, respectively. At the Ni/Mn layer, 4 reduced Ni^{2+} experience large oxidations to $4Ni^{(4-\Delta6)+}$. The charge states of Co and Mn cations are almost unchanged. For $x = 0.25 \rightarrow x = 0.125$, a large oxidation takes place for $4Ni^{3+}$ at the Ni/Ni layer, while a partial oxidation for $4Ni^{(4-\Delta5)+}$ and $4Ni^{(4-\Delta6)+}$ at the Ni/Co and Ni/Mn layer, respectively. Co cations also undergo oxidation. Mn cations that were slightly oxidized for $x = 0.50 \rightarrow x = 0.25$ are reduced back at $x = 0.125$. Co cations also undergo oxidation. Mn cations that were slightly oxidized for $x = 0.50 \rightarrow x = 0.25$ are reduced back at $x = 0.125$. Hybridization of $p(O)-e_g(Ni)$ orbitals is found to be larger at the Ni/Ni layer than Ni/Co and Ni/Mn layer. Chakraborty *et al.* have also proposed that an increase of Ni content in NCM enhances the O−TMs covalency.[46] In our calculations, we also find a slight hybridization of $p(O)-e_g(Co)$ and $p(O)-e_g(Mn)$ at $x = 0.25$, which it increases at $x = 0.125$. The strengthening of O−TMs covalency by charging has also been reported by Koyama *et al.*[47] and Yabuuchi *et al.*[48] Note that our calculated total DOS shows no band gap for NCM811, but we find the formation of hole-electrons on Ni cations with the delithiation. This is because there is a gap between valence band maximum and conduction band minimum of Ni^{3+} cations, in particular those at the Ni layer, for Li1.00NCM811. The Ni cations at Ni/Co and Ni/Mn layers behave different than those at the Ni/Ni layer, which is most likely due to the effect of Co and Mn and/or projection of *d* states on Ni cations. The electron-holes are found to be close to Li vacancies (see Fig. S9), which is due to the electrostatic reason.

The decrease in the lattice parameter *a* with delithiation (Fig. 1) is explained by the gradual shrinking of the ionic radius of Ni cations as well as suppression of J−T distortions in Ni−O octahedra. Note that the deviation from a linear relation between *a* and *x* at $x = 0.50$ is due to the H−M phase transition. The reason for the increase of *a* at $x = 0.125$ compared to $x = 0.25$ is probably due to the increase in in-plane electrostatic repulsion between TMs. Although the ionic radii of oxidized Ni^{3+} ions become smaller and their J−T distortions are suppressed, the ionic radius of oxidized Co^{4+} does not change much compared to Co^{3+}.[49] However, the electrostatic repulsion (along *a* and *b* directions) between Co^{4+} and other TMs increases. The non-monotonic change in the *c* value is due to the competition between O−Li−O and O−TM−O forces. Figure 4 (a) illustrates the averaged projected O−O distance on the *c* axis for the O−TM−O intralayer (d_1) and interlayer (d_2). In-plane distances between arbitrary Ni ions of different layers are shown in figure S10. To explain the behavior of *c*, we analyzed the variation of d_1 and d_2, which determine the *c* value to be $(d_1 + d_2) \times 3$. When $x = 1.00 \rightarrow x = 0.75$, d_1 decreases by 4.41 % due

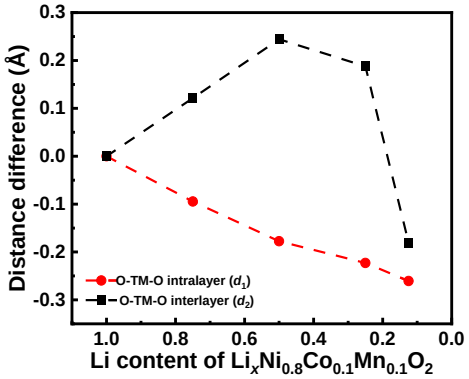

Figure 4. Projected O−TM−O intralayer (d_1) and O−TM−O intralayer (d_2) lengths on the *c* axis. Calculated d_1 and d_2 lengths at each layer are shown in bottom.

to the contraction of ionic radius of $4Ni^{3+} \rightarrow 4Ni^{(4-\Delta2)+}$ at the Ni/Ni layer, and $4Ni^{3+} \rightarrow 4Ni^{4+}$ at the Ni/Co layer, and $4Ni^{(3-\Delta1)+} \rightarrow 4Ni^{3+}$ at the Ni/Mn layer. However, d_2 increases by 4.70 % because of the disappearing of electrostatic attraction between removed Li ions and O anions. Our Bader charge calculation indicates that O anions are reduced slightly at the Ni/Ni layer but those at the Ni/Co and Ni/Mn layers are slightly oxidized (see Fig. S8 in SI). This indicates that changes in O−O electrostatic interaction plays a minor role in determining d_2. The magnitude of increase in d_2 is larger than that of decrease in d_1 leading to the expansion of *c*. Since changes in d_1 and d_2 are not very different from those for $x = 1.00 \rightarrow x = 0.75$, we obtain a similar expansion in the *c* lattice parameter for $x = 0.75 \rightarrow x = 0.50$. For $x = 0.50 \rightarrow x = 0.25$, the decrease in d_1 is 1.74 % smaller than that for $x = 0.75 \rightarrow x = 0.50$ ($\Delta d_1 = 4.05$ %). This behavior can be due to the presence of 4 J−T active Ni^{3+} at O−TM−O layers. On the other hand, d_2 shrinks by 2.00 %. Bader charge analysis indicates that O anions of all three layers are oxidized (see Fig. S8 in SI). In this case, the impact of vanishing partial Li−O electrostatic attraction seems to be weaker than that of the decrease in the strength of O−O interaction due to the oxidation of O anions. The decrease of both d_1 and d_2 causes the *c* value for NCM811 shrinks considerably. Finally, when $x = 0.125$, a contraction of d_1 by 1.96 % is observed. This decrease is due to the vanishing of J−T distortion for Ni cations. Moreover, a large contraction of d_2 is also obtained for $x = 0.25 \rightarrow x = 0.125$ which arises from a large O oxidation and sliding of O−TM−O layers with respect to each other. (The sliding effect will be discussed later.)

In comparison to NCM111,[33] the length of d_2 expands larger for $x = 1.00 \rightarrow x = 0.50$ in NCM811. When $x = 0.50 \rightarrow x = 0.25$, d_2 starts to decrease for NCM811, which is not observed for NCM111 when $x = 0.50 \rightarrow x = 0.33$. It is because of more oxidation of O for NCM811 with delithiation strengthening the O−O bonding forces. For $x = 0.25 \rightarrow x = 0.125$, the interlayer sliding in the NCM811, and thereby the decrease in the *c* value, is smaller than that in NCM111. This is despite the larger oxidation of O anions in the former case. The d_2 layer decreases with delithiation for both cases. However, a large shrink of d_2 is found when $x = 0.33 \rightarrow x = 0.17$ for NCM111 owing to the suppression of J−T distortion of all Ni^{3+} for NCM111.[33]

Figure 5 indicates that the H−M phase transition at $x = 0.50$ is related to the arrangement of Ni^{3+} and Ni^{4+} cations at the Ni/Ni layer. One half of NiO_6 octahedra undergoes local

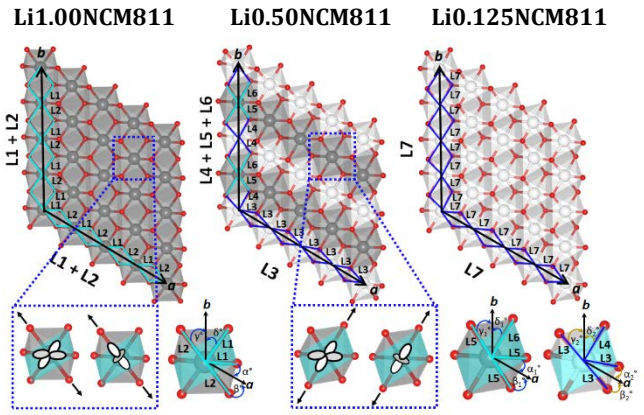

Figure 5. Top views of the Ni/Ni layer of NCM811 for different Li concentrations. $Ni^{(3\pm\Delta)+}$ and $Ni^{(4\pm\Delta)+}$ are in Grey and white, respectively. Calculated equatorial $Ni^{(3\pm\Delta)+}$–O (L1 and L5), axial $Ni^{(3\pm\Delta)+}$–O (L2 and L6), equatorial $Ni^{(4\pm\Delta)+}$–O (L3 and L7), axial $Ni^{(4\pm\Delta)+}$–O (L4 and L7) bond lengths have been discussed. The shape of NiO_6 octahedra (zoomed in) and orientation of *d* orbitals are shown in the bottom.

distortions due to the J-T effect of their Ni^{3+}, but the other half of octahedra with Ni^{4+} possess no local J-T distortion. A special ordering of $Ni^{3+}O_6$ and $Ni^{4+}O_6$ octahedra along *a* and *b* results in the H → M phase transition. It seems that the phase transition is dictated by the Ni/Ni layer. Due to an unequal number of NiO_6 octahedra with and without local distortions as well as existence of Co and Mn cations, a similar ordering as in the Ni layer is not expected in the other layers. This is in line with the observed H–M phase transition in LNO systems.[50] For x = 1.00 all Ni^{3+} cations at the Ni/Ni layer undergo the local J–T distortion, but the periodic sequence of projected Ni–O bond lengths (L1: half of the average equatorial O–Ni^{3+}–O length, L2: half of the average axial O–Ni^{3+}–O length) along *a* and *b* are similar. Therefore, Li1.00NCM811 has no collective J-T distortion and exhibits a hexagonal symmetry. At x = 0.50 where half Ni cations have charge states of 4+, all equatorial O–Ni^{4+}–O bond lengths, namely L3, are also similar and aligned along *a*. However, along *b*, the axial O–Ni–O bond length of Ni^{3+} (2L6) is larger than that of Ni^{4+} (2L4) as well as the equatorial O–Ni–O bond length of Ni^{3+} (2L5) and Ni^{4+} (2L3). In this case the projected length of sequential L3 over *a* direction is different from that of L4, L5, and L6 over *b*. The shorter bond length of L3 compared to L4, L5, and L6 causes the smaller *a* value in comparison to *b*. For the aforementioned reasons, a larger value is obtained for *b* in comparison to *a*. As a result, Li0.50NCM811 undergoes collective J-T distortion, leading to the H → M phase transition. At x = 0.125, where all Ni cations have charge states 4+, a similar projected O–Ni–O length over *a* and *b* is found since the axial and equatorial bond lengths of Ni^{4+}–O are almost equal leading to the alleviation of the H–M phase transition.

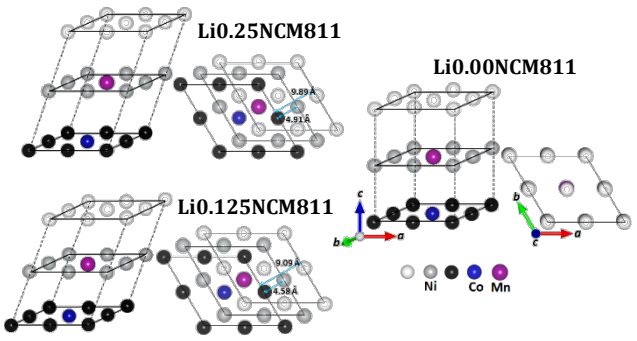

Figure 6. Side and top views of TM layers in the O3 phase of Li0.25NCM811 and Li0.125NCM811 as well as the O1 phase of Li0.00NCM811.

Furthermore, we studied the possibility of phase transition from O3 to O1 at deep delithation states which has been reported by Noh *et al.*,[16] Biasi *et al.*,[15] and Ryu *et al.*[50] Fig. 6 illustrates that the first and second O–TM–O layers (counted from the topmost layer) move in-plane direction towards the third O–TM–O layer. Our DFT-SCAN calculation shows that the O3 phase is more favorable than the O1 one at x = 0.125, even though a slight sliding of the O–TM–O layers with respect to each other is observed. However, the latter phase becomes more favorable at the fully-delithiated state. Moreover, we computed the total Coulomb energies of the DFT-SCAN calculated structures of O3 and O1 phases using both the Bader charges and formal charges (see Tab. S6 in SI). The results show that for both charge states, the O1 phase is more favorable than the O3 phase at x = 0.00. This is different from the NCM111 case in which only with Bader charges O1 is more favorable.[33] Nevertheless, for both NCM811 and NCM111, the Bader charges on ions are larger in the O1 phase than the O3 phase at x = 0.00.[33]

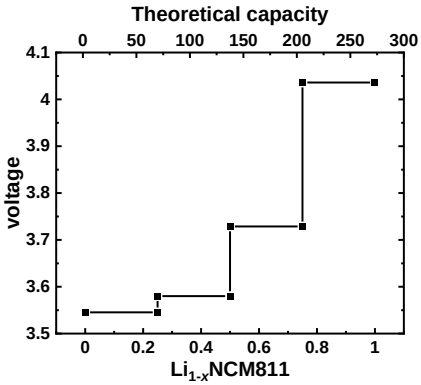

Figure 7. Calculated voltage for Li1-*x*NCM811 as function of 1-*x* and theoretical capacity.

Finally, we computed the voltage profile with

$$V = -\frac{E(\mathrm{Li}_{x+dx}\mathrm{NCM811}) - E(\mathrm{Li}_{x}\mathrm{NCM811})}{dx} + E(\mathrm{Li}),$$

where $E(\mathrm{Li}_{x+dx}\mathrm{NCM811})$ and $E(\mathrm{Li}_{x}\mathrm{NCM811})$ are the total energy per formula unit of the system before and after dx Li deintercalation, respectively. $E(\mathrm{Li})$ is the energy per formula unit of bulk metal Li. The Li0.125NCM811 structure was excluded from our calculation due to its (aforementioned) combined covalent-ionic nature of bonding. The variation of voltage with Li content is qualitatively in fair agreement with the experimental data by Biasi *et al.*[21] and Noh *et al.*[22] In particular, the simulated curve reproduces the larger increase in voltage for lower x values. Calculated voltages with DFT-SCAN are about 0.30-0.50 V higher than the experimental measurements,[21,22] which is definitely due to the exchange-correlational energy approximation in the DFT calculation. The

computed voltage values by Chakraborty *et al*. for LNO with DFT-SCAN is also lower than the corresponding experimental values.[32]

Conclusions

In this work, we modelled structural changes in Li*x*NCM811 with delithiation/lithiation *x*. The most favorable arrangements of TMs and Li ions were determined by performing extensive electrostatic energy analysis followed by DFT calculations. Our detailed analysis on local spin polarization, spin density difference, density of states, and Bader charges helped us to explain the reason behind non-monotonic variation of *a*, *b*, and *c*, and, in particular, structural phase transitions with *x*. It is found that (i) number of Li ions, (ii) charges on TMs and O, (iii) site preference of TMs, (iv) J−T distortion, and (v) electrostatic interactions are the main factors controlling lattice parameters and symmetry. The decreases in *a* for $x = 1.00 \rightarrow x = 0.25$ is controlled by the factors (ii) and (iv), while the increase in *a* for $x = 0.25 \rightarrow x = 0.125$ is due to the factor (ii) and (v). The increase in *c* for $x = 1.00 \rightarrow x = 0.50$ is controlled by factor (i). The removal of Li ions which act as glue between O−TM−O layers leads to the weakening of the O−Li−O attraction and thereby the expansion of *c*. The decrease in *c* for $x = 0.50 \rightarrow x = 0.25$ is due to the factors (ii) and (iv), and the sharp decrease in *c* for $x = 0.25 \rightarrow x = 0.125$ is induced by factors (ii) and (v). Whereas the H−M phase transition relies on factor (iii) and (iv). Co and Mn cations occupy TM sites such that every third layer comprises of only Ni cations. The length of axial axis in Ni^{3+}−O octahedra is larger than that in Ni^{4+}−O as well as that of equatorial axis in Ni^{3+}−O and Ni^{4+}−O octahedra at the Ni/Ni layer leading to the phase transition in NCM811 at $x = 0.50$. Finally, we showed that the O3 → O1 phase transition in the fully delithiated case is driven by factor (v). A similar H−M phase transition is expected for other Ni-rich NCM cathodes with at least one O−Ni−O layer. This is because the collective Jahn-Teller effect that was found in this work occurs probably in O−TM−O layers comprising of only Ni besides O.

ASSOCIATED CONTENT

Supporting Information. Atomic structures; calculated magnetizations; calculated Bader charges; estimation of charge states of TMs; calculated Coulomb energies.

AUTHOR INFORMATION

Corresponding Author

*Payam Kaghazchi − Forschungszentrum Jülich GmbH, Institute of Energy and Climate Research, Materials Synthesis and Processing (IEK-1), Jülich, D-52425, Germany; E-Mail: p.kaghazchi@fz-juelich.de

Authors

Olivier Guillon − Forschungszentrum Jülich GmbH, Institute of Energy and Climate Research, Materials Synthesis and Processing (IEK-1), Jülich, D-52425, Germany; E-Mail: o.guillon@fz-juelich.de

Liang-Yin Kuo − Physikalische und Theoretische Chemie, Freie Universität Berlin, Arnimallee 22, Berlin, D-14195, Germany; E-Mail: liangku16063@zedat.fu-berlin.de

Conflict of Interest

The authors declare no competing interests.

ACKNOWLEDGMENT

Authors gratefully acknowledge support from the "Bundesministerium für Bildung und Forschung" (BMBF) as well as the computing time granted through JARA-HPC on the supercomputer JURECA at Forschungszentrum Jülich.

REFERENCES

(1) Manthiram A. A reflection on lithium-ion battery cathode chemistry. *Nat. Commun.* **2020**, 11, 1550.

(2) Mizushima K.; Jones P. C.; Wiseman P. J.; Goodenough J. B. Li_xCoO_2 ($0 < x < 1$): A new cathode material for batteries of high energy density. *Mater. Res. Bull.* **1980**, 15, 783−798.

(3) Radin M. D.; Hy S.; Sina M.; Fang C.; Liu H.; Vinckeviciute J. *et al*. Narrowing the gap between theoretical and practical capacities in Li-Ion layered oxide cathode materials. *Adv. Energy Mater.* **2017**, 7, 1602888.

(4) Nitta N.; Wu F.; Lee J. T.; Yushin G. Li-ion battery materials: present and future. *Mater. Today* **2015**, 18, 252−264.

(5) Yano A.; Shikano M.; Ueda A.; Sakaebe H.; Ogumi Z. $LiCoO_2$ degradation behavior in the high-voltage phase transition region and improved reversibility with surface coating. J. Electrochem. Soc. **2017**, 164, A6116−A6122.

(6) Liu Q.; Su X.; Lei D.; Qin Y.; Wen J.; Guo F. *et al*. Approaching the capacity limit of lithium cobalt oxide in lithium ion batteries via lanthanum and aluminium doping. *Nat. Energy* **2018**, 3, 936−943.

(7) Xu J.; Lin F.; Doeff M. M.; Tong W. A review of Ni-based layered oxides for rechargeable Li-ion batteries. *J. Mater. Chem. A* **2017**, 5, 874−901.

(8) Kan W. H.; Huq A.; Manthiram A. Low-temperature synthesis, structural characterization, and electrochemistry of Ni-rich spinel-like $LiNi_{2-y}Mn_yO_4$ ($0.4 \leq y \leq 1$). *Chem. Mater.* **2015**, 27, 7729−7733.

(9) Kim J.-S.; Johnson C. S.; Vaughey J. T.; Thackeray M. M.; Hackney S. A.; Yoon W. *et al*. Electrochemical and structural properties of $xLi_2M'O_3\cdot(1-x)LiMn_{0.5}Ni_{0.5}O_2$ electrodes for lithium batteries (M' = Ti, Mn, Zr; $0 \leq x \leqslant 0.3$). *Chem. Mater.* **2004**, 16, 1996−2006.

(10) Chebiam R. V.; Kannan A. M.; Prado F.; Manthiram A. Comparison of the chemical stability of the high energy density cathodes of lithium-ion batteries. *Electrochem. Commun.* **2001**, 3, 624−627.

(11) Zheng Y.; Xu N.; Chen S.; Liao Y.; Zhong G.; Zhang Z. *et al*. Construction of a stable $LiNi_{0.8}Co_{0.1}Mn_{0.1}O_2$ (NCM811) cathode interface by a multifunctional organosilicon electrolyte additive. *ACS Appl. Energy Mater.* **2020**, 3, 2837−2845.

(12) Kim J.-H.; Park K.-J.; Kim S. J.; Yoon C. S.; Sun Y.-K. A method of increasing the energy density of layered Ni-rich $Li[Ni_{1-2x}Co_xMn_x]O_2$ cathodes ($x = 0.05, 0.1, 0.2$). *J. Mater. Chem. A* **2019**, 7, 2694−2701.

(13) Tang M.; Yang J.; Chen N.; Zhu S.; Wang X.; Wang T. *et al*. Overall structural modification of a layered Ni-rich cathode for enhanced cycling stability and rate capability at high voltage. *J. Mater. Chem. A* **2019**, 7, 6080−6089.

(14) Dixit M.; Markovsky B.; Schipper F.; Aurbach D.; Major D. T. Origin of structural degradation during cycling and low thermal stability of Ni-rich layered transition metal-based electrode materials. *J. Phys. Chem. C* **2017**, 121, 22628−22636.

(15) Li J.; Manthiram A.; A comprehensive analysis of the interphasial and structural evolution over long-term

cycling of ultrahigh-nickel cathodes in lithium-Ion batteries. *Adv. Energy Mater.* **2019**, 9, 1902731.
(16) Bianchini M.; Roca-Ayats M.; Hartmann P.; Brezesinski T.; Janek J. There and back again–The journey of $LiNiO_2$ as a cathode active material. *Angew. Chem. Int. Ed.* **2019**, 58 10434–10458.
(17) Märker K.; Reeves P. J.; Xu C.; Griffith K. J.; Grey C. P. Evolution of structure and lithium dynamics in $LiNi_{0.8}Mn_{0.1}Co_{0.1}O_2$ (NMC811) cathodes during electrochemical cycling. *Chem. Mater.* **2019**, 7, 2545–2554.
(18) Li W.; Asl H. Y.; Xie Q.; Manthiram A. Collapse of $LiNi_{1-x-y}Co_xMn_yO_2$ lattice at deep charge irrespective of nickel content in lithium-ion batteriesJ. *Am. Chem. Soc.* **2019**, 141, 5097–5101.
(19) Kondrakov A. O.; Geßwein O.; Galdina K.; de Biasi L.; Meded V.; Filatov E. O. *et al*. Charge-transfer-induced lattice collapse in Ni-rich NCM cathode materials during delithiationJ. *Phys. Chem. C* **2017**, 44, 24381–24388.
(20) Li J.; Downie L. E.; Ma L.; Qiu W.; Dahn J. R. Study of the failure mechanisms of $LiNi_{0.8}Mn_{0.1}Co_{0.1}O_2$ cathode material for lithium ion batteries. *J. Electrochem. Soc.* **2015**, 162, A1401–A1408.
(21) de Biasi L.; Kondrakov A. O.; Geßwein H.; Brezesinski T.; Hartmann P.; Janek J. Between scylla and charybdis: balancing among structural stability and energy density of layered NCM cathode materials for advanced lithium-ion batteries. *J. Phys. Chem. C* **2017**, 121, 26163–26171.
(22) Noh H.-J.; Youn S.; Yoon C. S.; Sun Y.-K.; Comparison of the structural and electrochemical properties of layered $Li[Ni_xCo_yMn_z]O_2$ (x = 1/3, 0.5, 0.6, 0.7, 0.8 and 0.85) cathode material for lithium-ion batteries. *J. Power Sources* **2013**, 233, 121–130.
(23) Chang K.; Hallstedt B.; Music D.; Thermodynamic description of the $LiNiO_2$–NiO_2 pseudo-binary system and extrapolation to the $Li(Co,Ni)O_2$–$(Co,Ni)O_2$ system. *Calphad* **2012**, 37, 100–107.
(24) Schipper F.; Dixit M.; Kovacheva D.; Talianker M.; Haik O.; Grinblat J. *et al*. Stabilizing nickel-rich layered cathode materials by a high-charge cation doping strategy: zirconium-doped $LiNi_{0.6}Co_{0.2}Mn_{0.2}O_2$. *J. Mater. Chem. A* **2016**, 4, 16073–16084.
(25) Dixit M.; Kosa M.; Lavi O. S.; Markovsky B.; Aurbach D.; Major D. T. Thermodynamic and kinetic studies of $LiNi_{0.5}Co_{0.2}Mn_{0.3}O_2$ as a positive electrode material for Li-ion batteries using first principles. *Phys. Chem. Chem. Phys.* **2016**, 18, 6799–6812.
(26) Min K.; Kim K.; Jung C.; Seo S.-W.; Song Y. Y.; Lee H. S. A comparative study of structural changes in lithium nickel cobalt manganese oxide as a function of Ni content during delithiation process. *J. Power Sources* **2016**, 315, 111–119.
(27) Liang C.; Longo R. C.; Kong F.; Zhang C.; Nie Y.; Zheng Y. *et al.* Site-dependent multicomponent doping strategy for Ni-rich LiNi1−2yCoyMnyO2 (y = 1/12) cathode materials for Li-ion batteries. *J. Power Sources*, **2017**, 340, 217–228.
(28) Perdew J. P.; Burke K.; Ernzerhof M. *Phys. Rev. Lett.* **1996**, 77, 3865–3868.
(29) Hubbard J. Electron correlations in narrow energy bands. *Phys. Eng. Sci.* **1963**, 276, 238–257.
(30) Grimme, S.; Antony, J.; Ehrlich, S.; Krieg, H. A consistent and accurate *ab initio* parametrization of density functional dispersion correction (DFT-D) for the 94 elements H-Pu. *J. Chem. Phys.* **2010**, 132, 154104.
(31) Sun J. W.; Ruzsinszky A.; Perdew J. P. Strongly constrained and appropriately normed semilocal density functional. *Phys. Rev. Lett.* **2015**, 115, 036402.
(32) Chakraborty A.; Dixit M.; Aurbach D.; Major D. T.; Predicting accurate cathode properties of layered oxide materials using the SCAN meta-GGA density functional. *npj Comput. Mater.* **2018**, 4, 60.
(33) Kuo L.-Y.; Guillon O.; Kaghazchi P. On the origin of non-monotonic variation of the lattice parameters of $LiNi_{1/3}Co_{1/3}Mn_{1/3}O_2$ with lithiation/delithiation: a first-principles study. *J. Mater. Chem. A* **2020**, 8, 13832–13841.
(34) Jung R.; Metzger M.; Maglia F.; Stinner C.; Gasteiger H. A.; Oxygen release and its effect on the cycling stability of $LiNi_xMn_yCo_zO_2$ (NMC) cathode materials for Li-Ion batteries. *J. Electrochem. Soc.* **2017**, 164, A1361–A1377.
(35) Blöchl P. E. Projector augmented-wave method. *Phys. Rev. B: Condens. Matter Mater. Phys.* **1994**, 50, 17953–17979.
(36) Kresse G.; Furthmüller J. Efficient iterative schemes for *ab initio* total-energy calculations using a plane-wave basis set. *Phys. Rev. B: Condens. Matter Mater. Phys.* **1996**, 54 11169–11186.
(37) Okhotnikov K.; Charpentier T.; Cadars S. Supercell program: a combinatorial structure-generation approach for the local-level modeling of atomic substitutions and partial occupancies in crystals. *J. Cheminformatics* **2016**, 8 17.
(38) Momma K.; Izumi F. VESTA 3 for three-dimensional visualization of crystal, volumetric and morphology data. *J. Appl. Crystallogr.* **2011**, 44, 1272–1276.
(39) Lim J.-M.; Hwang T.; Kim D.; Park M.-S.; Cho K.; Cho M. Intrinsic origins of crack generation in Ni-rich $LiNi_{0.8}Co_{0.1}Mn_{0.1}O_2$ layered oxide cathode material. *Sci. Rep.* **2017**, 7, 39669.
(40) Flores E.; Novak P.; Aschauer U.; Berg E. J. Cation ordering and redox chemistry of layered Ni-rich $Li_xNi_{1-2y}Co_yMn_yO_2$: An operando raman spectroscopy study. *Chem. Mater.* **2020**, 32, 186–194.
(41) Liang C.; Kong F.; Longo R. C.; KC S.; Kim J.-S.; Jeon S. *et al*. Unraveling the origin of instability in Ni-rich $LiNi_{1-2x}Co_xMn_xO_2$ (NCM) cathode materials. *J. Phys. Chem. C* **2016**, 120, 6383–6393.
(42) Park M. S. First-principles study of native point defects in $LiNi_{1/3}Co_{1/3}Mn_{1/3}O_2$ and Li_2MnO_3. Phys. Chem. Chem. Phys. **2014**, 16, 16798–16804.
(43) Koyama Y.; Tanaka I.; Adachi H.; Makimura Y.; Ohzuku T. Crystal and electronic structures of superstructural $Li_{1-x}[Co_{1/3}Ni_{1/3}Mn_{1/3}]O2$ ($0 \le x \le 1$). *J. Power Sources* **2003**, 119–121, 644–648.
(44) Saadoune I.: Ménétrier M.; Delmas C. Redox processes in $Li_xNi_{1-y}Co_yO_2$ cobalt-rich phases. *J. Mater. Chem.* **1997**, 7, 2505–2511.
(45) Chebiam R. V.: Kannan A. M.; Prado F.; Manthiram A.; Comparison of the chemical stability of the high energy density cathodes of lithium-ion batteries. *Electrochem. Commun.* **2001**, 3, 624–627.
(46) Chakraborty A.; Kunnikuruvan S.; Dixit M.; Major D. T.; Review of computational studies of NCM cathode materials for Li-ion batteries. *Isr. J. Chem.* **2020**, 60, 850–862.
(47) Koyama Y.; Yabuuchi N.; Tanaka I.; Adachi H.; Ohzuku T. Solid-state chemistry and electrochemistry of $LiCo_{1/3}Ni_{1/3}Mn_{1/3}O_2$ for advanced lithium-ion batteries: I. first-principles calculation on the crystal and electronic structures. *J Electrochem. Soc.* **2004**, 151, A1545.
(48) Yabuuchi N.; Makimura Y.; Ohzuku T. Solid-state chemistry and electrochemistry of $LiCo_{1/3}Ni_{1/3}Mn_{1/3}O_2$ for advanced lithium-ion batteries: III. rechargeable capacity and cycleability. *J Electrochem. Soc.* **2007**, 154, A314.

(49) Shannon R. D. Revised effective ionic radii and systematic studies of interatomic distances in halides and chalcogenides. *Acta Crystallogr A.* **1976**, 32, 751–767.
(50) Ryu H.-H.; Park K.-J.; Yoon C. S.; Sun Y.-K.; Capacity fading of Ni-rich $Li[Ni_xCo_yMn_{1-x-y}]O_2$ ($0.6 \le x \le 0.95$) cathodes for high-energy-density lithium-ion batteries: bulk or surface degradation? *Chem. Mater.* **2018**, 30, 1155–1163.

Abstract Graphic

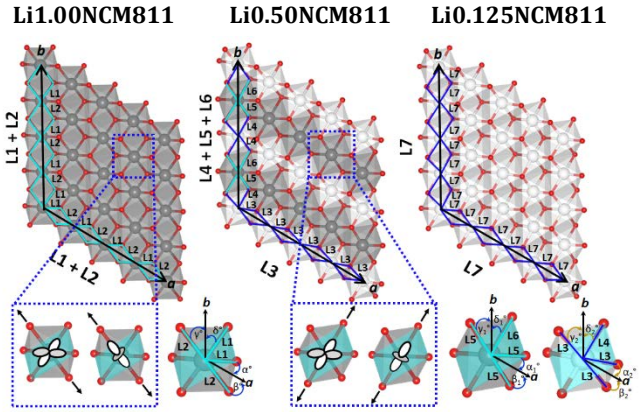

Synopsis Structural phase transitions in NCM811 are modelled and explained by combining electrostatic analysis and DFT calculations.